CONF-960306--31

PRELIMINARY ASSESSMENT OF THE EFFECTS OF BIAXIAL LOADING ON REACTOR PRESSURE VESSEL STRUCTURAL-INTEGRITY-ASSESSMENT TECHNOLOGY

W. E. Pennell, B. R. Bass, J. W. Bryson,
T. L. Dickson, W. J. McAfee, and J. G. Merkle
Oak Ridge National Laboratory
Oak Ridge, Tennessee 37831

ABSTRACT*

Effects of biaxial loading on shallow-flaw fracture-toughness have been investigated to determine their potential impact on the structural integrity assessment of a reactor pressure vessel (RPV) under, (a) pressurized-thermal-shock (PTS) transient loading, and (b) pressure-temperature (P-T) loading produced by the reactor heat-up and cool-down transients. Biaxial shallow-flaw fracture-toughness test results were also used to determine the parameter controlling fracture in the transition temperature range, and to develop a related dual-parameter fracture-toughness correlation. Shallow-flaw and biaxial loading effects were found to reduce the conditional probability of crack initiation by a factor of nine when the shallow-flaw fracture-toughness K_{Jc} data set, with biaxial-loading-effects adjustments, was substituted in place of the American Society of Mechanical Engineers (ASME) Code K_{Ic} data set in PTS analyses. Biaxial loading was found to reduce the shallow-flaw fracture-toughness of RPV steel such that the lower-bound curve was located between the ASME K_{Ic} and K_{IR} curves. This finding has relevance to any future development of the P-T curve analysis procedures. Fracture in the shallow-flaw biaxial specimens tested at temperatures in the lower transition temperature range was shown to be strain controlled. A strain-based dual-parameter fracture-toughness correlation was developed and shown to be capable of predicting the effect of crack-tip constraint on fracture-toughness for strain-controlled fracture.

* Research sponsored by the Office of Nuclear Regulatory Research, U.S. Nuclear Regulatory Commission under Interagency Agreement 1886-8084-5B with the U.S. Department of Energy under Contract DE-AC05-96OR22464.

1. INTRODUCTION

Pressure loading and thermal gradient loading both produce biaxial stress fields in the pressure boundary of a reactor pressure vessel (RPV). Pressure loading produces a stress field with a ratio of longitudinal-stress/hoop-stress (σ_L/σ_H) of 0.5, whereas thermal gradient loading typically produces an equibiaxial stress field with a σ_L/σ_H ratio of 1.0. It follows that the stress-field-biaxiality ratios of interest for structural integrity assessments of the RPV pressure boundary under combined pressure and thermal loading are in the range $0.5 \leq \sigma_L/\sigma_H \leq 1.0$. This paper provides a very preliminary assessment of the effect of σ_L/σ_H ratios in this range on analysis procedures, either currently in use or under consideration, for assessing the structural integrity of an RPV pressure boundary containing flaws. The assessment is necessarily very preliminary because of the limited biaxial-effects fracture-toughness data available at this time.

2. APPLICATIONS

Two loading cases are of primary interest for the structural integrity assessment of an RPV pressure boundary. These are (a) pressurized-thermal-shock (PTS) transient loading, and (b) pressure-temperature (P-T) loading produced by the reactor heat-up and cool-down transients. Biaxial loading effects on shallow-flaw fracture-toughness have the potential to influence the structural integrity assessment of an RPV for both of these loading cases. In addition, the controlled application of biaxial loading produces shallow-flaw fracture-toughness results with controlled variations in crack-tip constraint. Data from biaxial tests are, therefore, particularly valuable when applied to the development and validation of dual-parameter fracture-toughness correlations for application at transition-range temperatures normalized to the reference nil-ductility temperature ($T\text{-}RT_{NDT}$).

DISCLAIMER

2.1 PRESSURIZED THERMAL SHOCK

A typical biaxial stress field produced in the RPV pressure boundary by PTS transient loading is shown in Fig. 1, together with a constant depth shallow surface flaw. Thermal stresses are highest adjacent to the inner surface of the vessel where the effects of irradiation embrittlement and transient temperatures combine to produce a maximum reduction in the material fracture-toughness. The net result of this combination of conditions is that the majority of crack initiations predicted in a probabilistic PTS analysis originate from shallow flaws located on the inner surface of the vessel.

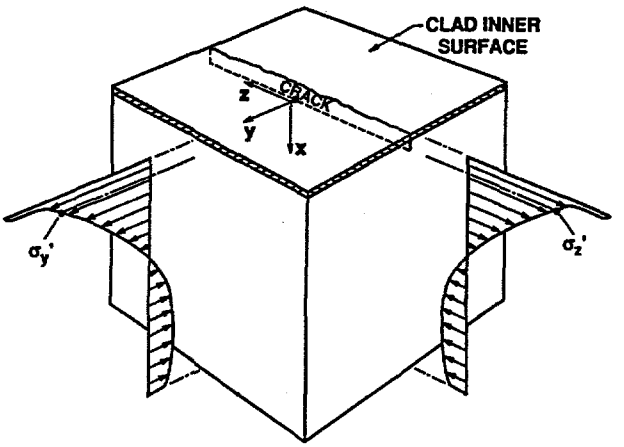

Fig. 1. PTS loading biaxial stresses in a reactor vessel wall with one of the principal stresses aligned parallel with the tip of a constant-depth shallow surface flaw

One of the principal stresses in Fig. 1 is seen to be aligned parallel to the crack front of a shallow surface flaw. There is no counterpart of this far-field out-of-plane stress in fracture-toughness tests performed using single-edge-notched-bend (SENB) test specimens with uniaxial loading. Shallow-flaw fracture-toughness of RPV material has been shown to be higher than the deep-flaw fracture-toughness because of the relaxation of crack-tip constraint. The far-field out-of-plane stress has the potential to increase stress triaxiality (constraint) at the crack-tip, and thereby reduce the shallow-flaw fracture-toughness enhancement. Effects of biaxial-loading must, therefore, be factored into any future application of shallow-flaw fracture-toughness data to the probabilistic analysis of RPV integrity under PTS loading. Requirements for the evaluation of RPV integrity under PTS loading are given in Ref. 1, and guidelines for implementation of those requirements are provided in Ref. 2.

2.2 REACTOR VESSEL P-T CURVES

A typical P-T envelope for an RPV is shown in Fig. 2. Surveillance program data are used to periodically adjust the upper bound to the reactor P-T operating envelope,[3,4,5] which is controlled by the fracture-toughness of the RPV material. Adjustment is required to maintain margins against fracture of two on pressure loading and one on simultaneously applied thermal loading. Fracture prevention margins are calculated assuming an inner surface flaw, having a depth corresponding to one quarter of the wall thickness ($\frac{1}{4}$t), and a surface-length of 1 $\frac{1}{2}$t. Selection of this flaw size was, in part, a reflection of the limited capability of the nondestructive examination (NDE) technology available at the time the P-T curve requirements were defined. The fracture margin assessment analysis must be performed using lower-bound dynamic fracture-toughness properties (K_{IR}).[3] This requirement reflects a concern that fracture could originate from local brittle zones in the vessel and propagate in a dynamic manner to the $\frac{1}{4}$t depth.

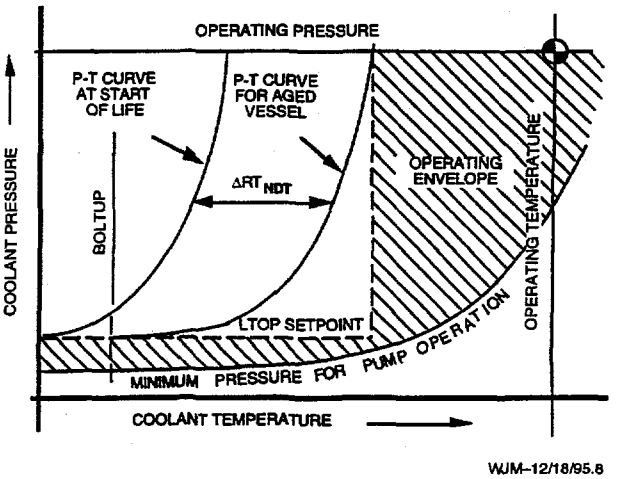

Fig. 2. Adjustment of the reactor P-T curve in response to irradiation embrittlement of the vessel material severely restricts the permitted reactor operating envelope

Adjustment of the P-T curve in response to irradiation embrittlement of the reactor vessel material has the effect of restricting the permissible reactor P-T operating envelope, as illustrated in Fig. 2. The upper bound to the P-T envelope is defined by the vessel material P-T curve, modified by the operating characteristics of the low temperature overpressure protection (LTOP) system as required by Section 5.2.2 of the U.S. Nuclear Regulatory Commission (USNRC) Standard Review Plan.[6] The lower bound of the P-T envelope is set by the pressure required at a given temperature to prevent cavitation of the main coolant pumps.

It is evident from Fig. 2 that a high irradiation-induced ΔRT_{NDT} can restrict the permissible reactor P-T operating envelope to the point where reactor heat-up (outside flaw critical) and cool-down (inside flaw critical) become very difficult operations. This is particularly true for reactors with a fixed setpoint LTOP system. This difficulty has sparked interest in refinement of the technology used to define the P-T curve and the associated LTOP setpoint. Developments which have been discussed in the nuclear-power plant community include, (a) replacing the current $\frac{1}{4}$t flaw with a smaller flaw, and (b) substituting a less restrictive fracture-toughness curve in place of the K_{IR} curve. The admissibility of these potential changes is a regulatory issue and will not be discussed further here.

The case for reducing the reference flaw size rests on demonstrated improvements in the detection and sizing performance of modern NDE systems, while the case for adjusting the fracture-toughness curve derives from recent studies of pop-ins and local brittle zones[7] which indicate that

they do not significantly degrade the material fracture-toughness. It is appropriate to note, however, that shallow-flaw fracture-toughness considerations must be addressed in any future evaluation of the potential changes discussed above. The effect of biaxial loading on shallow-flaw fracture-toughness will be an important element of that evaluation.

2.3 DUAL-PARAMETER FRACTURE TOUGHNESS CORRELATIONS

Fracture initiates when limiting stress or strain conditions are exceeded at the tip of a crack. Stress-induced fracture initiates in a brittle material when the opening-mode stress exceeds a critical value over a finite length.[8] Strain-induced fracture initiates when crack-tip strains exceed the stress-state-dependent ductility of the material.[9-14] Crack-tip stress fields can be divided into hydrostatic and shear components. Yielding of the material, and the crack-tip blunting deformation that post-yield plastic deformation can produce, is governed by the shear component of the stress field. Tensile hydrostatic stresses contribute directly to the opening-mode tensile stresses but do not influence yielding or crack-tip blunting. It follows, therefore, that fracture-toughness under stress-limiting conditions will be directly influenced when the hydrostatic component of the crack-tip stress field increases. Strain-controlled fracture-toughness will be similarly influenced by increases in the hydrostatic component of the crack-tip stress field because of reduced crack-tip blunting, which increases the crack-tip strain concentration. Crack-tip constraint is the term used to describe conditions that influence the hydrostatic component of the crack-tip stress field.

Dual-parameter fracture-toughness corrections and correlations have been proposed to provide a quantitative assessment of the effect of reduction of crack-tip constraint on fracture-toughness. These include the J-A_{cr} fracture-toughness correction proposed by Dodds, Anderson and Kirk[15] and the J-Q dual parameter fracture-toughness correlation proposed by O'Dowd and Shih.[16,17] These dual-parameter fracture-toughness corrections and correlations share a common feature in that they each utilize the effect of crack-tip constraint on the in-plane stresses at the crack tip to infer the effect of constraint on fracture-toughness.

In the J-Q fracture-toughness correlation, Q defines the departure of the hydrostatic component of the opening-mode stress distribution on the crack plane from the opening-mode stress distribution derived by Hutchinson,[18] Rice, and Rosengren[19] (HRR) for a highly constrained crack tip. Ritchie, Knott, and Rice[8] (RKR) have proposed a criterion relating the critical value of the crack-tip opening-mode tensile stress for the onset of cleavage fracture in mild steel under plane-strain constraint conditions. The J-Q fracture-toughness correlation uses the RKR concept of a critical opening-mode tensile stress, together with the influence of constraint, represented by the parameter Q, on opening-mode stresses to correlate the effect of crack-tip constraint on fracture-toughness.

Prior investigations of biaxial loading effects have concluded that out-of-plane biaxial loading had no effect on in-plane stresses at the crack tip, but did influence the width of the crack-tip plastic zone in the direction of crack propagation.[20,21] Recent elastic-plastic finite element analyses of the Oak Ridge National Laboratory (ORNL) biaxial specimen by Bryson and Bass,[22] using a model with a highly refined treatment of the crack-tip region, have confirmed these conclusions (see Fig. 3). The Bryson-Bass analyses[22] have further confirmed that the stress-based J-A_{cr} constraint correction cannot predict the observed effects of biaxial loading on shallow-flaw fracture-toughness (see Fig. 4). The Heavy-Section Steel Technology (HSST) program has, therefore, investigated the utility of a strain-based constraint-effects correlation.

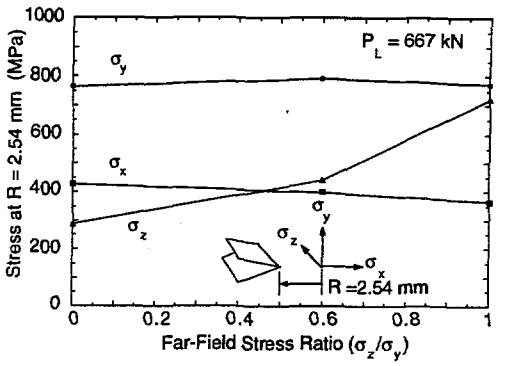

Fig. 3. Far-field stress biaxiality has little effect on the in-plane stresses near the crack tip

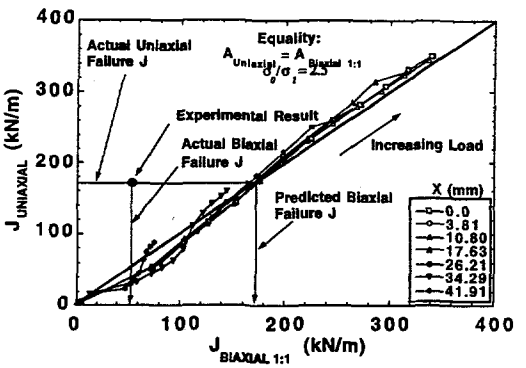

Fig. 4. Validation check on the Dodds-Anderson constraint adjustment for data from biaxial (P_T/P_L - 1.0) and uniaxial (P_T/P_L = 0.0) tests

The case for development of a strain-based dual parameter correlation for transition range fracture-toughness derives from results produced by a number of constraint-related research activities. Clausing[12] showed that the plane-strain ductility of structural steels increases rapidly over a relatively small temperature range, corresponding with the fracture-toughness transition temperature range. Clausing related the decrease in toughness associated with increase in strength to the associated decrease in plane-strain ductility. Barsom[13] and Merkle[14] developed expressions for K_{Ic} based upon plane-strain ductility. The expressions of Refs. 13 and 14 produced K_{Ic} predictions, for temperatures in the transition range, which matched the test data. Weiss[23] developed an equation for fracture-toughness based upon the stress-state-dependent material fracture strain. An adaptation of the Weiss equation was used in the scoping analysis of Ref. 21 to determine the potential impact of biaxial loading on fracture-toughness. The

scoping analysis of Ref. 21 predicted a K_{JcB}/K_{JcU} ratio of 0.47 for equibiaxial loading, where K_{JcB} and K_{JcU} are values of K from J for biaxial and uniaxial loading conditions, respectively. This compares with the lower-bound K_{JcB}/K_{JcU} ratio of 0.57 obtained in tests with equibiaxial and uniaxial loading. Similarity of the predicted and measured K_{JcB}/K_{JcU} values is supportive of a strain-based fracture-toughness correlation. Fractographic data from examinations of broken fracture specimens[24,25] provides further support for a strain-based fracture-toughness correlation. The fractographic data indicate that many crack initiation sites are located in the region of the crack tip process zone where strain is increasing, but stress is decreasing, with increasing applied K_J.

It will be evident from the above brief review of the development of dual-parameter fracture-toughness correlations that, (a) stress-based dual-parameter correlations cannot predict the observed effects of biaxial loading on transition-range shallow-flaw fracture-toughness, (b) this problem with stress-based dual-parameter correlations became evident only when biaxial hallow-flaw fracture-toughness data became available, (c) strain-based dual-parameter correlations are required if crack-tip constraint effects are to be factored into predictions of transition-range shallow-flaw fracture-toughness behavior, and (d) biaxial shallow-flaw fracture-toughness test data and analyses are essential to the development and validation of a strain-based dual parameter fracture-toughness correlation.

3. FRACTURE TOUGHNESS DATA

3.1 SHALLOW-FLAW FRACTURE TOUGHNESS DATA

Fracture toughness tests have been performed on SENB test specimens using both deep (a/W = 0.5) and shallow (a/W = 0.1) flaws.[26, 27] Beam specimens used in these tests are shown in Fig. 5 and 6. The beams tested by ORNL (Fig. 5) were fabricated from A 533 Grade B Class 1 (A 533 B) material and were nominally 100 mm deep. Beams with a 230 mm square cross section (Fig. 6) were cut from the reactor vessel from a canceled nuclear plant and tested, under an HSST program subcontract, by the National Institute for Standards and Technology (NIST). The inner-surface stainless steel cladding remained in place on the large scale test beams tested by NIST, and the flaws were located in the reactor vessel longitudinal welds. Additional shallow-flaw fracture-toughness data for A 533 B material were generated by the Fatigue and Fracture Branch of the Naval Surface Warfare Center (NSWC), in Annapolis, Maryland.[28] Material for the NSWC tests was heat treated to increase its yield stress. The NSWC tests were also conducted using large (B = 89 mm, W = 83 mm) SENB specimens. Use of large-scale beams permitted testing of shallow flaws with depths in the range identified as critical for PTS analysis. Data from Refs. 26, 27, and 28 were all generated using large-scale SENB specimens fabricated from RPV steel. They can, therefore, be combined into deep-flaw and shallow-flaw data sets.

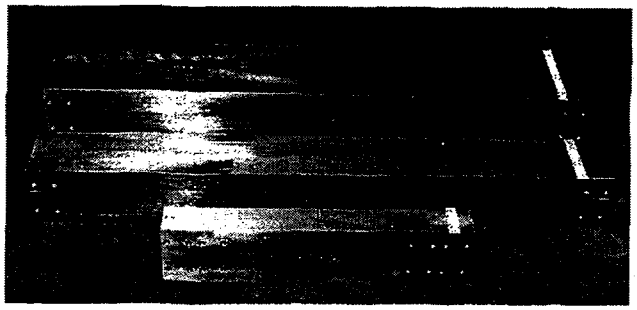

Fig. 5. 100-mm-deep beams were used in the shallow-flaw test program to permit full-scale testing of surface flaws having depths in the range which PTS analysis has shown to be the controlling range for crack intrusion

Fig. 6. A limited number of full scale beam specimens were used in the shallow-flaw test program. The specimens were cut from the shell of a reactor pressure vessel from a canceled nuclear plant

The reference temperature for nil-ductility transition (RT_{NDT}) is used as a normalizing parameter for fracture-toughness data. The ASME Boiler and Pressure Vessel Code[29] defines RT_{NDT} in terms of both the nil-ductility temperature (NDT) and the temperature (T_{Cv}) at which the lower bound Charpy energy from 3 tests is not less than 68-J (50 ft-lb). One of the temperatures (NDT or T_{Cv}) will be the controlling temperature for RT_{NDT} in a given situation. A mix of governing conditions is contained within the data sets from NSWC, ORNL, and NIST. Within a data set, NDT and RT_{NDT} are identical in the NSWC tests, and in the ORNL tests on the Combustion Engineering (CE) material. RT_{NDT} is higher than NDT for the ORNL tests on material from HSST Plate 13B and for the NIST tests on weld metal, indicating that T_{Cv} controlled RT_{NDT} in those cases.

Deep-flaw and shallow-flaw fracture-toughness data generated in these tests are plotted as functions of the normalizing temperature RT_{NDT} in Figs. 7 and 8, respectively. Open points and solid points in these plots represent data from material where RT_{NDT} was controlled by NDT and T_{Cv}, respectively. The deep flaw open and solid data points in Fig. 7 form a homogeneous group, indicating that RT_{NDT} is a satisfactory normalizing parameter for deep-flaw data. In contrast, the open-point and solid-point shallow-flaw data in Fig. 8 appear to belong to two separate families, with quite separate lower-bound curves. The apparent existence of two separate families of data for a single material calls into question the adequacy of RT_{NDT} as a normalizing parameter for the shallow-flaw fracture-toughness of A 533 B plate and weld material.

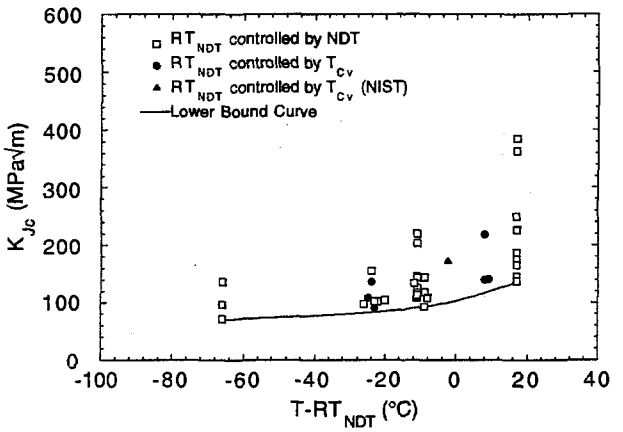

Fig. 7. The parameter controlling RT_{NDT} has no significant effect on the distribution of K_{Jc} vs T-RT_{NDT} data points from the deep-crack SENB A533B specimens. A single curve adequately defines the lower bound for the combined data set

Tests used to determine NDT and T_{Cv} are fundamentally different in character, and this difference could influence the interpretation, shown in Fig. 8, of the shallow-flaw fracture-toughness data. This problem can be eliminated by adopting a common basis for the normalizing parameter used to compare the data sets. This has been done in Fig. 9, where NDT has been used as the normalizing parameter for all data points. Figure 9 shows that the shallow-flaw fracture-toughness data from all sources form a homogeneous population when plotted as a function of T-NDT. A single curve defines the lower bound to the shallow-flaw fracture-toughness data sets. A comparison of Figs. 7 and 9 shows that the lower-bound curves for the deep- and shallow-flaw data are similar, but the mean fracture-toughness and scatter of data are significantly higher for shallow flaws than for deep flaws.

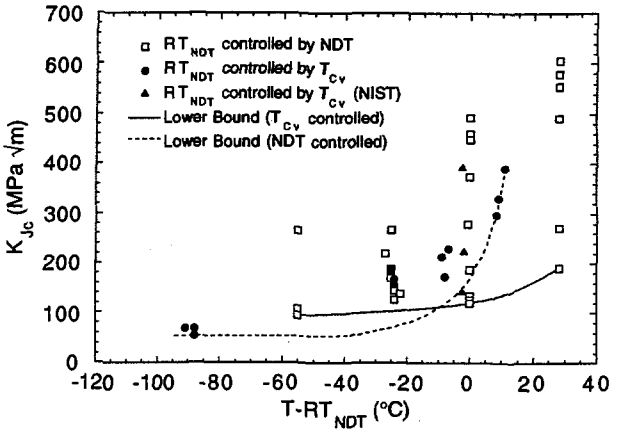

Fig. 8. Shallow-flaw fracture toughness data for A533B plate and weld material fall into two distinct groups when plotted as a function of the normalizing parameter T-RT_{NDT}. The groups are characterized by the parameter controlling RT_{NDT} (NDT or T_{Cv})

The data of Fig. 9 were used to generate the baseline RPV structural integrity analysis results presented in Section 4. The baseline results were then used as the basis-of-comparison for assessing the effects of biaxial loading on RPV integrity structural evaluations. This approach permitted a quantitative assessment of the effects of biaxial loading on the results. Direct evaluation of the effects of biaxial loading on RPV structural integrity evaluations made using the deep-flaw-based ASME Code fracture-toughness curves was not possible because matching deep-flaw-based biaxial fracture-toughness data are not available. Where appropriate, however, analyses performed using the ASME Code fracture-toughness curves and associated data are included to provide a basis for assessing the deep-flaw/shallow-flaw effects on the analysis results.

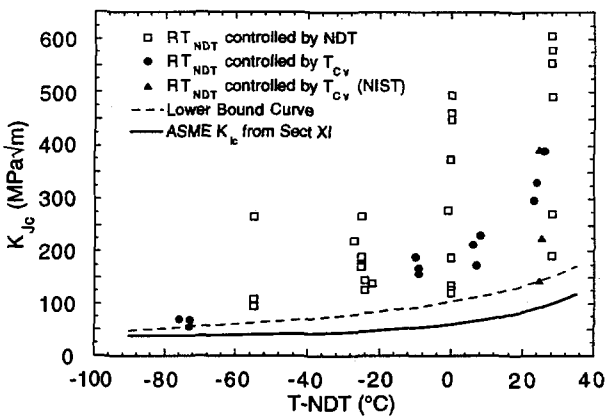

Fig. 9. Shallow-flaw fracture toughness data for A533B plate and weld material from a single homogeneous group when plotted as a function of the normalizing parameter T-NDT. The lower bound curve of this data set is similar to that of the deep flaw data set, but the shallow-flaw data set show an increase in both mean toughness and data scatter

3.2 BIAXIAL LOADING FRACTURE TOUGHNESS DATA

An initial series of biaxial tests has been completed using test specimens of the cruciform design shown in Fig. 10. The specimens were fabricated from a single heat of A 533 B material. The biaxial load ratio is defined as P_T/P_L, where P_T is the total load applied to the transverse beam arms and P_L is the total load applied to the longitudinal arms. Tests were run with P_T/P_L ratios of 0.0, 0.6, and 1.0. Details of those tests have been extensively reported,[24, 30] and will not be repeated here. K_{Jc} data from the biaxial tests are shown in Fig. 11, plotted as functions of the biaxiality ratio P_T/P_L. The plot shows a decrease in the lower-bound shallow-flaw fracture-toughness with increasing biaxiality ratios. The data also indicate a trend of decreasing data scatter at a stress ratio of 0.6 when compared with the data scatter observed in both the uniaxial ($P_T/P_L = 0$) SENB shallow-flaw tests (see Fig. 9) and the biaxial shallow-flaw tests at a P_T/P_L loading biaxiality ratio of 1.0.

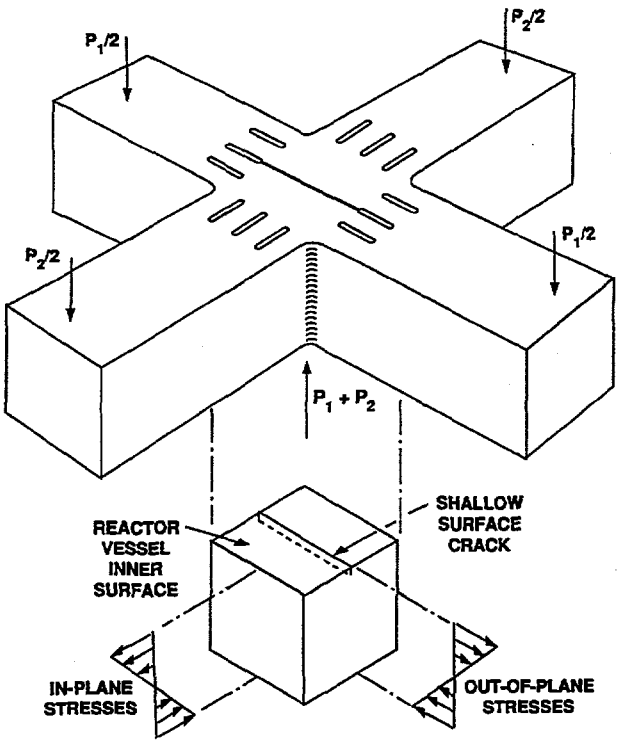

Fig. 10. Conceptual features of the cruciform shallow-flaw biaxial fracture toughness test specimen

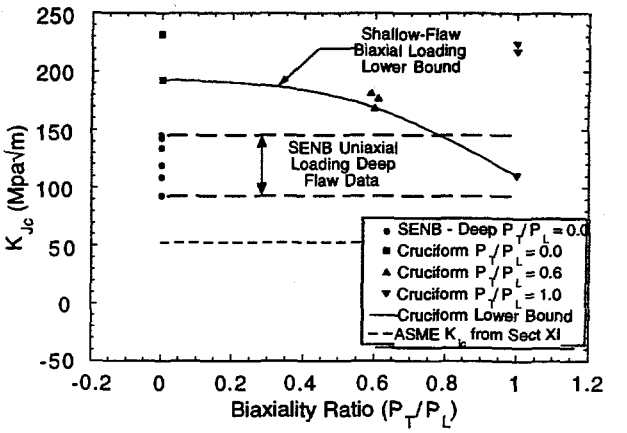

Fig. 11. Data from a single heat of A533B steel tested at T-NDT = -10°C indicate that biaxial loading reduces the lower-bound transition-range shallow-flaw fracture toughness

The biaxial specimens were all tested at normalized test temperatures in the range -11°C ≤ T-NDT ≤ -6°C.[22] A basis exists, therefore, for adjustment of the uniaxial shallow-flaw fracture-toughness curves for biaxial effects at normalized temperatures in the same range. It was necessary to estimate the effects of biaxial loading on shallow-flaw fracture-toughness at normalized test temperatures beyond this range in order to generate the biaxial-loading impact assessments. The assumption was made, therefore, that the percentage decrease in lower-bound shallow-flaw fracture-toughness produced by biaxial loading remained constant over the normalized temperature range of interest.

Deep flaw data from uniaxial tests conducted at normalized temperatures in the range T-NDT = -10°C ± 10°C on SENB specimens fabricated from the CE material are also shown in Fig. 11 at a P_T/P_L ratio of 0.0. Projection of the scatter band for these data to a $P_T/P_L = 1.0$ shows that the scatter bands for uniaxial-deep-flaw and biaxial-shallow-flaw data overlap.

4. BIAXIAL LOADING EFFECTS ON RPV INTEGRITY ASSESSMENTS

4.1 REACTOR VESSEL PTS ANALYSIS

Probabilistic fracture mechanics (PFM) analyses were performed to determine the sensitivity of the conditional probability of crack initiation, designated as P(I|E), to the effects of biaxial loading. The assessment is very preliminary because of the limited number of experimental shallow-flaw biaxial fracture initiation toughness data points available at this time. The assessment does not attempt to include a variational relationship between flaw depth and biaxial effects.

To perform PFM analyses, it was necessary to define mean-, upper-, and lower-bound fracture- initiation-toughness curves. In the Monte Carlo analysis process, for each simulated initial flaw depth, fracture-initiation toughness is stochastically sampled. There is not a sufficient number of experimental shallow-flaw biaxial K_{JC} data points from which to derive a statistically meaningful mean K_{JC} curve. For the purpose of performing these PFM sensitivity analyses, statistically

derived lower-bound and mean curves from the shallow-flaw uniaxial K_{Jc} database were adjusted, based on the limited biaxial data, to account for biaxial effects.

Figure 12 illustrates the shallow-flaw uniaxial K_{Jc} database and the statistically derived mean curve. The K_{Jc} data were generated by HSST program tests conducted at ORNL, NIST and NSWC. The data from the shallow-flaw testing program were generated for SENB shallow flaw specimens of A 533 B plate material and submerged arc pressure vessel weld material. This fracture initiation-toughness database was generated for uniaxial loading and therefore does not include the effects of biaxial stress fields. Primary characteristics of this fracture-initiation- toughness database are a higher mean value and increased variability, particularly in the transition region, relative to the database from which the ASME Code fracture-initiation-toughness curve was derived.

The equation for the statistically derived mean curve for the shallow-flaw uniaxial K_{JcU} database is

$$(K_{JcU}) \text{ mean} = 233.8 \times 10^{[0.0062073(T\text{-}NDT)]} \quad (1)$$

where the units for K_{JcU} and T-NDT are in MPa$\sqrt{m}$ and °C, respectively.

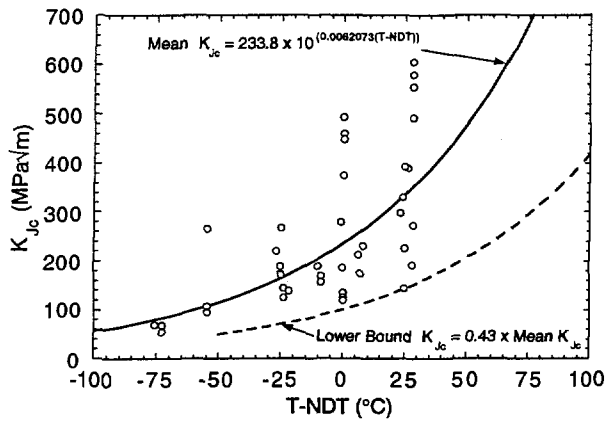

Fig. 12. Mean and lower bound K_{Jc} curves derived from the uniaxial shallow-flaw fracture toughness data and used in the RPV PTS analysis

Figure 12 also shows a lower-bound curve for the shallow-flaw uniaxial database that was established by shifting the mean curve down by 57%. In Fig. 12, the lower-bound curve is truncated since values of (T-NDT) below -50°C are not relevant to these analyses. An upper-bound curve was established by shifting the mean curve up by an equal 57 percent. This upper-bound curve, which does not envelope all of the shallow-flaw uniaxial data, was used for simplicity in these PFM analyses. The equations for the lower and upper-bound curves for the shallow-flaw uniaxial K_{Jc} database, respectively are:

$$(K_{JcU}) \text{ lower-bound} = 0.43 \times (K_{JcU}) \text{ mean} \quad (2)$$

$$(K_{JcU}) \text{ upper-bound} = 1.57 \times (K_{JcU}) \text{ mean} \quad (3)$$

As discussed in Section 2.3, a lower-bound K_{JcB}/K_{JcU} ratio of 0.57 was obtained in HSST program tests with uniaxial and biaxial loading. Therefore, the lower-bound curve for shallow-flaw biaxial loading was established by shifting (K_{JcU}) lower-bound down by 43 percent. The resulting shallow-flaw biaxial lower-bound K_{Jc} curve is shown in Fig. 13. For reference, Fig. 13 also includes the ASME K_{Ic} curve. Based on biaxial data in Fig. 11, an upper-bound shallow-flaw biaxial curve was derived by adjusting the shallow-flaw uniaxial upper-bound curve down by 3 percent. The mean curve for shallow-flaw biaxial loading was taken as equidistant between the lower- and upper-bound curves. Therefore, the equations for lower- and upper-bound and mean fracture initiation curves for shallow-flaw biaxial loading, respectively, are:

$$(K_{JcB}) \text{ lower-bound} = 0.57 (K_{JcU}) \text{ lower-bound} = 0.25 (K_{JcU}) \text{ mean} \quad (4)$$

$$(K_{JcB}) \text{ upper-bound} = 0.97 (K_{JcU}) \text{ upper-bound} = 1.52 (K_{JcU}) \text{ mean} \quad (5)$$

$$(K_{JcB}) \text{ mean} = 0.89 (K_{JcU}) \text{ mean} \quad (6)$$

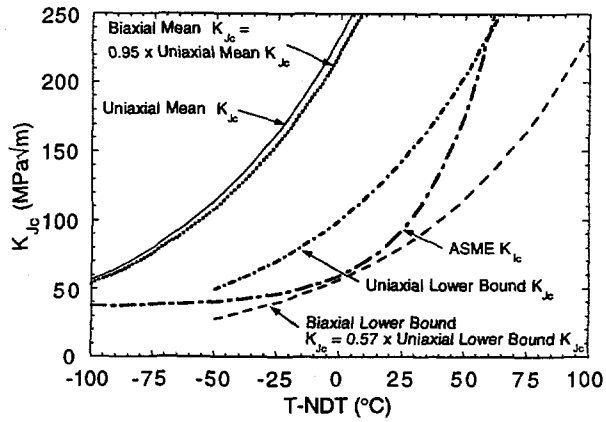

Fig. 13. Mean and lower-bound K_{Jc} curves adjusted to reflect the effect of P_T/P_L - 1.0 loading biaxiality on shallow-flaw fracture toughness

The FAVOR code[31] was utilized to perform PFM analyses for a PWR with prototypical geometry and thermo-elastic material properties. PFM analyses were performed for two transients. The first was the Calvert Cliffs transient identified as transient 8.3 in the Integrated Pressurized Thermal Shock Program (IPTS).[32] The second transient was the PTS benchmark transient utilized in the Nuclear Regulatory Commission/Electric Power Research Institute co-sponsored PTS benchmarking exercise.[33] The latter thermal transient is characterized by a stylized exponentially decaying coolant temperature. The following formulation is used for the exponentially decaying thermal transient:

$$T(t) = T_f + (T_i - T_f) \exp(-ß \bullet \text{time}) \quad (7)$$

where,

T(t) = coolant temperature at time t (min) in °C,
T_i = coolant temperature at time = 0 (°C),

T_f = final coolant temperature (°C), and

ß = exponential decay constant (min^{-1}).

For the PTS benchmark transient, the final coolant temperature is 66°C (150°F). The exponential decay constant, ß, is 0.15 min^{-1}. The initial coolant temperature is 288°C (550°F). The pressure is constant and is equal to 6.9 MPa (1.0 ksi).

The Calvert Cliffs transient 8.3 is illustrated in Fig. 14. It is characterized by a severe repressurization. Repressurization was the single most distinguishing characteristic of the so-called dominant transients (those transients that made significant contributions to the total frequency of vessel failure) analyzed in the IPTS studies.[32,34,35]

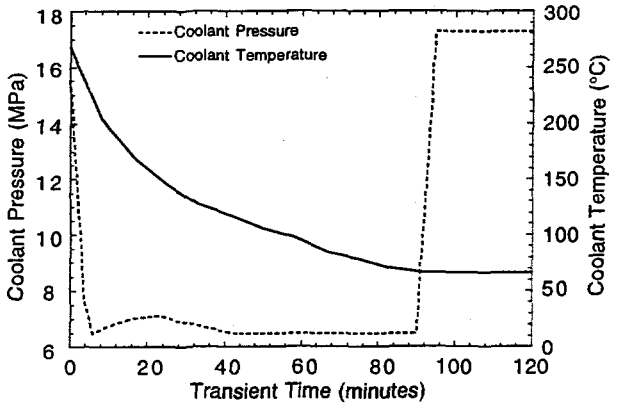

Fig. 14. The Calvert Cliffs PTS transient 8.3 includes severe repressurization

All PFM analyses performed in this study were for an infinite-length axially oriented weld assumed to contain exactly one flaw. Three PFM analyses were performed for each of the two transients described above, using the fracture initiation toughness correlations described below:

- The ASME K_{Ic} curve was defined as the mean - 2σ K_{Ic} curve. The value of one standard deviation (1σ) was 0.15 (K_{Ic}) mean. This is the methodology utilized in the IPTS studies.[32,34,35]
- The uniaxial-fracture-initiation toughness curves as defined above and illustrated in Fig. 13 were used. The value of one standard deviation (1σ) was 0.29 (K_{JcU}) mean.
- The biaxial fracture initiation toughness curves as defined above and illustrated in Fig. 13 were used. The value of one standard deviation (1σ) was 0.32 (K_{JcB}) mean.

Fracture initiation toughness was sampled from a normal Gaussian distribution between -2σ and +2σ in these PFM analyses. Figure 15 illustrates the sensitivity of P(IIE) to the three fracture initiation toughness correlations for the PTS benchmark transient. The value of RT_{NDTs} is the value of RT_{NDT} at the inner surface of the vessel calculated according to Regulatory Guide 1.99, Revision 2.[36] The value of RT_{NDTs} + 2σ includes an uncertainty allowance of 15°C (59°F). The P(IIE) calculated using the biaxial K_{Ic} correlation is reduced by a factor of approximately 15, relative to using the ASME-based K_{Ic} correlation, evaluated at the PTS screening criterion of RT_{NDTs} + 2σ = 132°C (270°F).

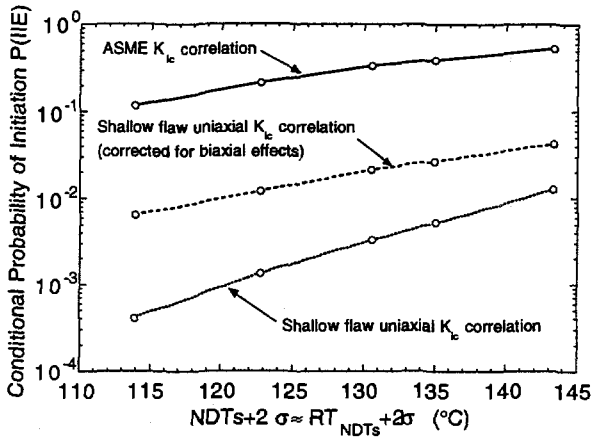

Fig. 15. Conditional probability of crack initiation for an infinite-length axial flaw in an RPV loaded by stylized PTS transient with T_f - 66°C (150°F), a decay constant of 0.15, and a constant 6.895 MPa (1.0 ksi) pressure

Fig. 16 illustrates the sensitivity of P(IIE) to the three fracture initiation correlations for the Calvert Cliffs transient 8.3. The P(IIE) calculated using the biaxial K_{Ic} correlation is reduced by a factor of approximately nine, relative to using the ASME-based K_{Ic} correlation, evaluated at the PTS screening criterion of RT_{NDTs} + 2σ = 132°C (270°F).

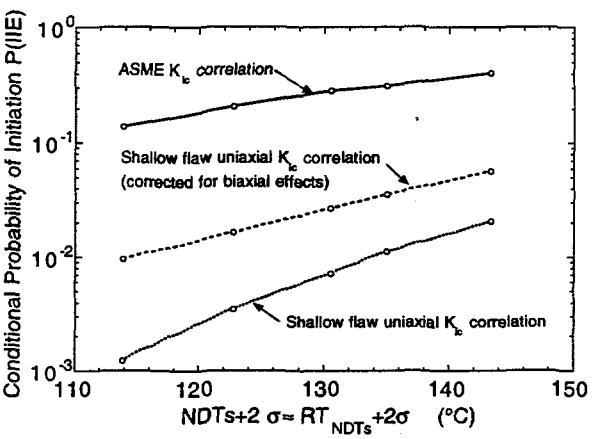

Fig. 16. Conditional probability of crack initiation for an infinite-length axial flaw loaded by a severe repressurization PTS transient (Calvert Cliffs 8.3)

4.2 REACTOR VESSEL P-T CURVE

Shallow-flaw-based fracture-toughness curves may find application in future development of the rules governing

determination of a reactor vessel P-T curve. Evaluation of the available shallow-flaw uniaxial and biaxial fracture-toughness data for RPV material provides a basis for assessing the potential impact of such a change. In this evaluation, the ASME Code K_{Ic} and K_{IR} fracture-toughness curves are used as a frame of reference for a potential shallow-flaw fracture-toughness curve.

Biaxial loading (P_T/P_L) effects on the shallow-flaw fracture-toughness of A 533 B material at a normalized temperature (T-NDT) of -10°C are shown in Fig. 11. Only the lower-bound biaxial results are used in this evaluation because the higher values of K_{Jc} obtained under equibiaxial loading (P_T/P_L = 1.0) were found by analysis to be associated with loss of contained yielding, a condition which is not relevant to the P-T curve application. The lower-bound (lowest measured) values for biaxiality ratios of P_T/P_L = 0.0 and 1.0 are shown in Table 1. The ratio of biaxial to the uniaxial fracture-toughness under otherwise identical conditions is defined as the biaxiality factor (BF). For the case of equibiaxial loading of shallow flaws, the biaxiality factor is obtained as BF = 110/193=0.57.

An adaptation of the ASME K_{Ic} curve is shown in Fig. 9 together with the shallow-flaw fracture-toughness data points. The adaptation of the ASME curve involved substitution of T-NDT in place of T-RT_{NDT} as the normalizing temperature. The lower bound to the shallow-flaw fracture-toughness data was generated by applying a factor F to the ASME K_{Ic} curve (where F is a linear function of T-NDT) such that the resulting curve passed through the lower-bound data points at T-NDT = -73°C and +24°C. The lower-bound data point at T-NDT = 24°C was obtained from shallow-flaw tests on a full-scale SENB test specimen cut from the RPV from a canceled nuclear plant. The shallow-flaw in this particular test was located in the longitudinal weld of the shell segment. NDT for this material was -50°C and the test temperature was -26°C. Characterization tests on the weld metal at -25°C showed its yield stress to be 600 MPa (87 ksi).[27] The high, but prototypical, yield stress for the weld material may have been responsible for the low shallow-flaw fracture-toughness value obtained in this test. The effect of biaxial loading was assessed at a normalized temperature of 24°C because this temperature is in the range of primary interest with respect to the P-T curve.

The lower-bound shallow-flaw K_{JcU} and the ASME K_{Ic} values at T-NDT = 24°C are given in Table 1. The estimated lower-bound shallow-flaw fracture-toughness at this temperature is obtained as follows

$$K_{JcB} = BF \cdot K_{JcU}, \text{ and} \quad (8)$$

$$K_{JcB} = 0.56 \cdot 144 = 81 \text{ MPa}\cdot\sqrt{\text{m}}. \quad (9)$$

K_{JcU} and K_{JcB} are shown plotted, together with the adapted ASME Code K_{Ic} and K_{IR} curves, in Fig. 17. K_{JcB} is located between the K_{Ic} and K_{IR} curves. The inference from this result is that the fracture-toughness curve included in any future proposal for adjustment of the P-T curve analysis procedures is anticipated to be below the Code K_{Ic} curve. Additional shallow-flaw uniaxial and biaxial fracture-toughness data on multiple heats of material and covering a range of normalized temperatures would be required to define that curve.

TABLE 1 APPLICATION OF CORRECTION FACTORS FROM THE BIAXIAL TEST PROGRAM TO TEST DATA FROM THE UNIAXIAL SENB TESTS PRODUCES ESTIMATED K_{JcB} FRACTURE-TOUGHNESS VALUES WHICH ARE MARGINALLY LOWER THAN THE ASME CODE K_{IC} VALUES AT A NORMALIZED TEMPERATURE IN THE LOWER TRANSITION RANGE.

			Fracture-Toughness ($MPa\sqrt{m}$)		
Test Specimen and Loading Condition	Flaw Depth/ Beam Depth (a/W)	T-NDT (°C)	ASME Code K_{Ic}	Test Data K_{Jc}	Estimated K_{Jc} with Biaxial Adjustment
Cruciform P_T/P_L=0.	0.12	-6	57	193	110
Cruciform P_T/P_L=1.	0.12	-8	56	110	110
Full Scale Uniaxial SENB	0.11	24	92	144	82

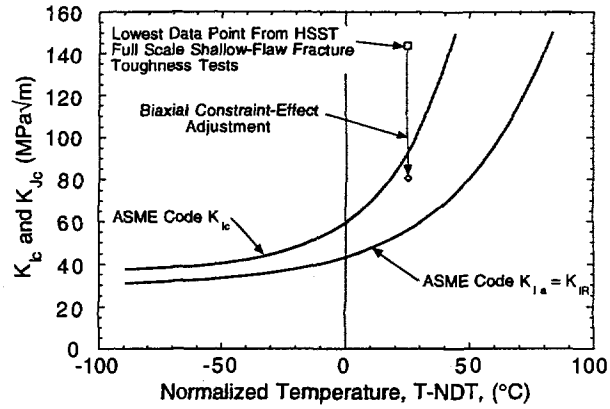

Fig. 17. The lowest data point from the full-scale uniaxial shallow-flaw fracture-toughness tests on weld material is located below the ASME K_{Ic} curve but above the K_{IR} curve when adjusted for the possible effects of biaxial loading

4.3 FRACTURE-TOUGHNESS CONSTRAINT-EFFECTS CORRELATIONS

Wells[9,10] and Tetelman and McEvily (T-M)[11] proposed that initiation of cleavage fracture is controlled by strains in the crack-tip region reaching a critical value. According to the T-M criterion, plastically induced fracture initiates in a ligament immediately adjacent to the blunted crack tip when the ligament strain reaches the fracture strain (ε_f) of the material. Wells[9] argued that the conditions at fracture can be characterized by a

critical crack-tip opening displacement (δ_c). As previously noted herein, a second (or dual) correlation parameter must also be introduced into the cleavage fracture model to quantify loss-of-constraint or departure from small-scale yielding conditions. Recent interpretations of the strain-based models by Pennell et al.[37] concluded that effects of constraint on fracture-toughness can be quantified by analyzing the response of crack-tip material to the applied load and by determining the effects of ligament strain fields on crack-tip deformation. However, direct application of the latter strain-based approach would require a finite-strain elastic-plastic finite element analysis to determine the crack-tip deformation as a function of strain fields in the ligament. To circumvent this computationally intensive approach, an alternative methodology was proposed that utilizes R_{pl}, the plastic zone width in the plane of the crack, as a second correlation parameter for fracture-toughness.[37]

The case for using R_{pl} in a strain-based fracture-toughness correlation derives from the observation that the crack-tip opening displacement (δ) is a function of the plastic zone width R_{pl} and that this relationship is constraint-dependent. The T-M formulation[11] can be shown to give a linear relationship between δ and R_{pl} for the case of plane-stress boundary conditions and contained yielding. The δ vs R_{pl} relationship for the more general beyond-plane-strain boundary conditions, for both contained and uncontained yielding, has been investigated using test data and analysis results from the HSST biaxial testing program.

The results for crack-mouth opening displacement (CMOD) from biaxial test data, together with results from 3-D finite-strain elastic-plastic finite-element analyses of the test specimens performed by Bryson and Bass, are summarized in Table 2. Estimates for δ at cleavage fracture for each of the biaxial tests were derived using results from Table 2 in the following proportional relationship,

$$\delta = \frac{CMOD \bullet (Lc - a)}{Lc} \qquad (10)$$

where

Lc = distance of the center of rotation (the point of stress reversal) from the tensile surface of the test specimen (mm), and

a = crack depth determined from examination of the test specimen fracture surface (mm).

TABLE 2 TEST DATA AND ANALYSIS RESULTS FROM THE SHALLOW-FLAW BIAXIAL TEST SPECIMENS

Test	Biaxial Load Ratio P_T/P_L	CMOD (mm)	Rotation Center Depth, Lc (mm)	$\sqrt{\delta_c}$ $(\sqrt{mm})$	Plastic Zone Width, R_{pl} (mm)	ln (R_{pl}) (R_{pl} in m)	Fracture Toughness K_{Jc} (MPa $\sqrt{m}$)
BB2	0.0	0.82	47.75	0.80	25.22	-3.68	232
BB11	0.0	0.70	46.48	0.74	24.23	-3.72	193
BB4	0.6	0.47	47.50	0.61	2.11	-6.16	177
BB5	0.6	0.51	47.50	0.63	2.29	-6.08	182
BB10	1.0	0.29	47.24	0.48	0.64	-7.35	110
BB7	1.0	0.75	47.75	0.77	24.72	-3.70	217
BB9	1.0	0.76	47.75	0.77	24.72	-3.70	224

A δ_c vs R_{pl} relationship was determined from 3-D finite element analysis of the biaxial test results at cleavage fracture initiation and is given by

$$\sqrt{\delta_c} = 1.043 + 0.073 \times \ln\left(R_{pl}\right). \qquad (11)$$

The linear relationship between $\sqrt{\delta_c}$ and $\ln(R_{pl})$ given by Eq. (11) is shown in Fig. 18, together with fracture-toughness data points obtained from the cruciform specimens. In Fig. 19, the $\sqrt{\delta}$ vs $\ln(R_{pl})$ loading trajectories are depicted for three biaxial loading ratios (i.e., P_T/P_L = 0, 0.6, and 1) applied to the cruciform specimen. These trajectories were generated using δ values computed from Eq. (10), with Lc, CMOD, and R_{pl} provided by results from 3-D finite-element analyses of the cruciform specimen. Unlike the $\sqrt{\delta_c}$ vs $\ln(R_{pl})$ toughness relationship of Fig. 18, the $\sqrt{\delta}$ vs $\ln(R_{pl})$ trajectories in Fig. 19 are strongly nonlinear and constraint dependent through the biaxial loading ratio. A noteworthy feature of the loading trajectory for P_T/P_L = 1 is the very rapid development of uncontained yielding at a point beyond which the trajectory follows the path for uniaxial loading, P_T/P_L = 0.

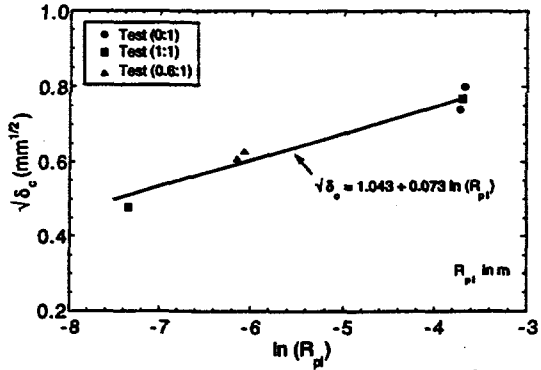

Fig. 18. Analyses of cruciform data imply $\sqrt{\delta_c}$ is linearly related to ln (R_{pl})

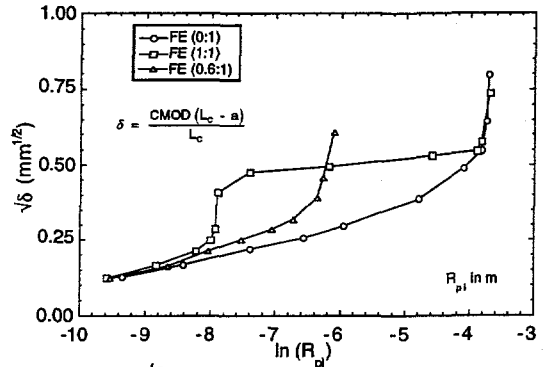

Fig. 19. The $\sqrt{\delta}$-ln(Rpl) loading trajectories are nonlinear and strongly dependent on biaxiality ratio (δ obtained from CMOD relation)

In Fig. 20, the range of fracture-toughness values possible at T- NDT = -10°C, for a given loading condition, is predicted by the intersection of the $\sqrt{\delta}$ vs ln(R_{pl}) loading trajectories with the $\sqrt{\delta_c}$ vs ln(R_{pl}) fracture-toughness locus of Fig. 18. Intersection of these nonlinear trajectories with the linear toughness locus is governed by the dependence of the trajectories on constraint as influenced by the biaxial loading ratio. Unique toughness values are predicted for the uniaxial (P_T/P_L=0) and biaxial (P_T/P_L=0.6) loading cases. The intersection of the trajectory for equibiaxial (P_T/P_L=1) loading with the toughness locus predicts both low and high toughness values for this loading condition. In fact, these low and high toughness values were realized in tests of the biaxial (P_T/P_L=1) loading case. The latter toughness data are shown in Fig. 11 expressed in terms of K_{Jc} values. Uncontained yielding that developed in two of the biaxial (P_T/P_L=1) tests gave high toughness values that were similar to those of the uniaxial loading tests. Collectively, the results depicted in Figs. 18-20 confirm that ln(R_{pl}) is a viable second parameter for characterizing strain-controlled fracture. This is an important observation because the parameter R_{pl} is relatively easy to calculate, making the resulting dual-parameter fracture-toughness correlation easy to use.

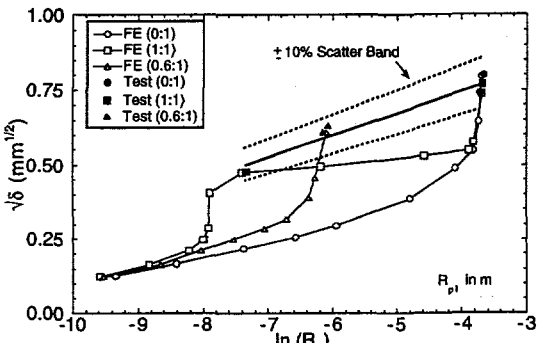

Fig. 20. Intersections of nonlinear $\sqrt{\delta}$ - ln (Rpl) loading trajectories with linear $\sqrt{\delta_c}$ - ln (R_{pl}) toughness locus are strongly dependent on biaxiality ratio

The fracture-toughness locus and loading trajectories given in Fig. 20 can be restated in terms of stress-intensity factors using the linear relationship between K_J and $\sqrt{\delta}$. Analysis results presented in Fig. 21 demonstrate that linearity of the K_J vs $\sqrt{\delta}$ relationship is preserved under the full range of biaxial loading ratios. Figure 22 depicts the equivalent K_J, K_{Jc} vs ln(R_{pl}) relationships for the cruciform testing program.

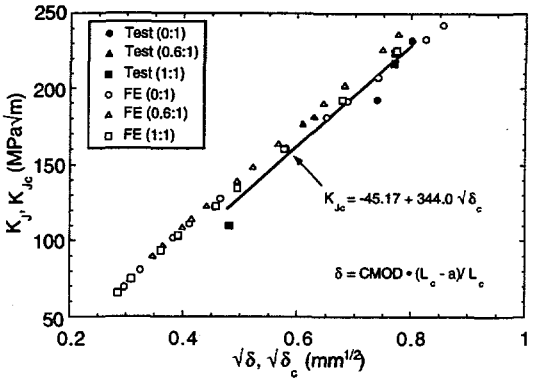

Fig. 21. The linear relationship between K_J and $\sqrt{\delta}$ is maintained for all biaxial loading ratios

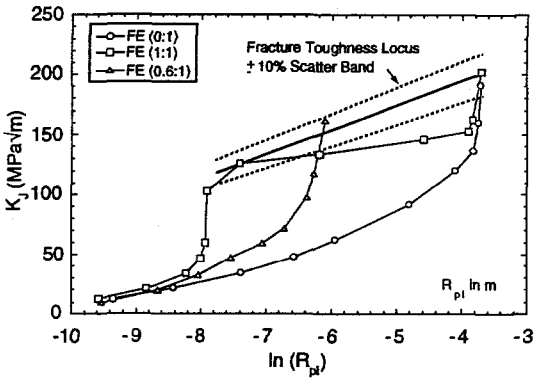

Fig. 22. Equivalent K_J , K_{Jc} vs ln (Rpl) relationships for cruciform testing program

Parameters that potentially could correlate the variations of loading trajectory with biaxial loading ratio depicted in Fig. 19 were studied using concepts discussed by Wells.[10] He employed a strip-yield model to study the hypothesis that initiation of brittle fracture is uniquely determined by a critical value of δ. For plane stress conditions, he developed relationships between δ, R_{pl}, and overall plastic strain, for loading conditions that range from below to above general yielding. Beyond general yielding, he postulated that δ becomes proportional to the plastic strain taken over some gauge length spanning the fully plastic area of the specimen. The objective herein was to determine which (if any) of the various stress and strain measures could be used to differentiate among the applied biaxial loading ratios to predict the $\sqrt{\delta}$ vs ln(R_{pl}) loading trajectories given in Fig. 19. Initial studies focused on the strip-yield Dugdale model and evaluations of stress-based parameters. In Barsom and Rolfe,[38] δ at the tip of the physical crack in the Dugdale model is given by the equation

$$\delta = \frac{8\bar{\sigma}a}{\pi E} \ln\left(1 + \frac{R_{pl}}{a}\right) \qquad (12)$$

where

$\bar{\sigma}$ = σ_{ys}, the yield stress in tension.

The Eq. (12) was used to predict $\sqrt{\delta}$ vs $\ln(R_{pl})$ loading trajectories corresponding to biaxial loading ratios of P_T/P_L = 0 and 1.0 for the loading sequences and R_{pl} values given in Table 2. Additional parameters required by Eq. (12) are σ_{ys} = 380 MPa (55 ksi), E= 189655 MPa (27500 ksi), and a = 10 mm (0.4 in). The resulting trajectories depicted in Fig. 23 essentially coincide for the full range of loading and do not exhibit the biaxial effect observed in Fig. 19. These calculations were repeated with the yield stress in Eq. (12) replaced by integral measures (i.e., an integrated average) of the opening-mode stress, σ_{33}, and the von Mises effective stress, σ_{eff}, taken over the plastic zone width,

$$\bar{\sigma} = \frac{1}{R_{pl}} \int_0^{R_{pl}} \sigma_{33}\, dr \qquad (13)$$

and

$$\bar{\sigma} = \frac{1}{R_{pl}} \int_0^{R_{pl}} \sigma_{eff}\, dr \qquad (14)$$

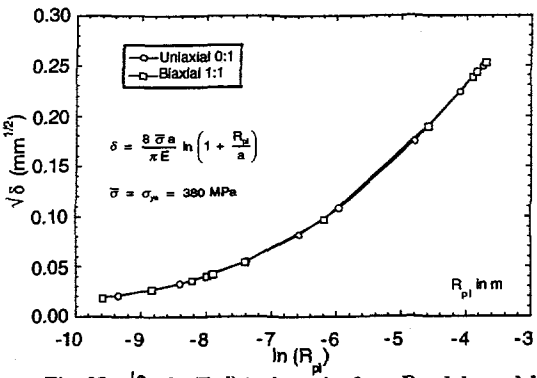

Fig. 23. $\sqrt{\delta}$ - ln (Rpl) trajectories from Dugdale model using a constant yield stress (380 MPa) do not detect effects of biaxiality ratio

Results corresponding to the two integral measures represented by Eqs. (13) and (14) are given in Figs. 24 and 25, respectively. Again, no significant effect of biaxial loading is discernable in the loading trajectories.

Given that the Dugdale model was not effective in predicting the loading trajectories of Fig. 19, attention was given next to a modified form of a δ relation due to Wells,[10]

$$\delta = \pi \bar{\varepsilon} R_{pl} \qquad (15)$$

where

$$\bar{\varepsilon} = \frac{1}{R_{pl}} \int_0^{R_{pl}} \varepsilon_{33}\, dr \qquad (16)$$

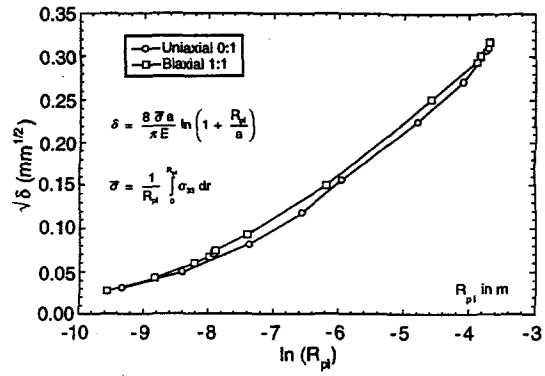

Fig. 24. $\sqrt{\delta}$ - ln (Rpl) trajectories from Dugdale model using an integrated average value of opening mode stress do not detect effects of biaxiality ratio

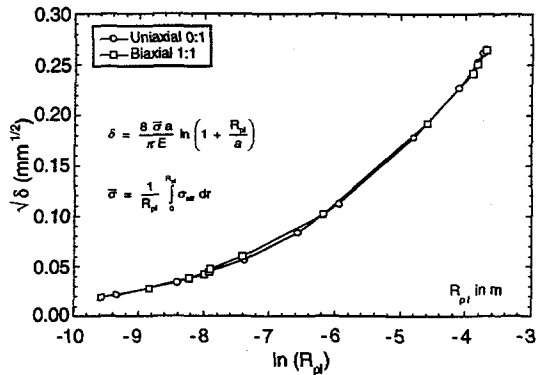

Fig. 25. $\sqrt{\delta}$ - ln (Rpl) trajectories from Dugdale model using an integrated average value of von Mises effective stress do not detect effects of biaxiality ratio

In Eq. (15), the integrated average of the opening-mode strain, $\bar{\varepsilon}$, taken over the plastic zone width, R_{pl}, replaces a quantity that Wells[10] defined as the overall tensile strain. Variations of $\bar{\varepsilon}$ *with longitudinal load, obtained from 3-D finite-element* analysis of three biaxial loading cases, P_T/P_L = 0, 0.6, and 1, are given in Fig. 26. These $\bar{\varepsilon}$ vs load relations were used in Eq. (15), along with calculated values of R_{pl}, to compute the predicted loading trajectories given in Fig. 27. Loading trajectories based on the CMOD relation, Eq. (10), are included in Fig. 27 for comparison. Overall, the trajectories computed from the $\bar{\varepsilon}$ relation are in good agreement with those obtained from the CMOD relation. At higher loads, the CMOD-derived trajectories are lower than those based on the $\bar{\varepsilon}$ relation, primarily due to reduced accuracy of Eq. (10) for the higher loads. The δ estimate provided by Eq. (10) is based on simple linear geometric relationships that do not account for an increased increment in δ due to crack-tip blunting at higher loads. However, these results confirm that a measure of the opening-mode strain field in the near-crack-tip ligament is capable of differentiating among the applied biaxial loading ratios to predict variations in biaxial loading trajectories.

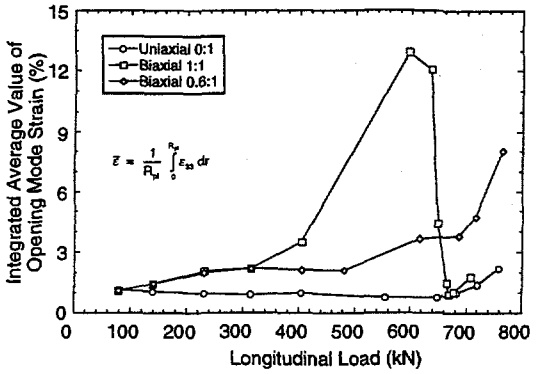

Fig. 26. Variation of integrated average value of opening mode strain with load is strongly dependent on biaxiality ratio

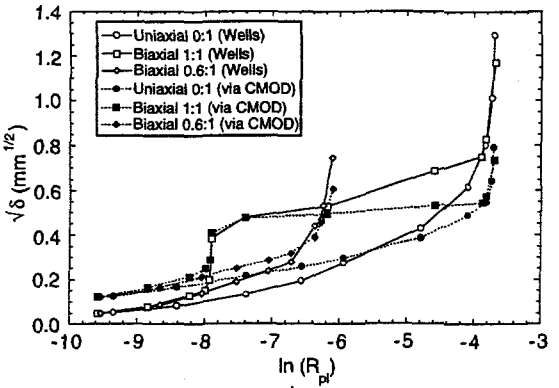

Fig. 27. Comparison of $\sqrt{\delta}$ - ln (Rpl) trajectories from simple geometric CMOD relation and from modified Wells relation

5. INTERIM CONCLUSIONS

Shallow-flaw and biaxial-loading effects on the conditional probability of RPV failure were determined for a stylized PTS transient and one of the dominant transients for the Calvert Cliffs nuclear plant. The conditional probability of crack initiation was reduced by a factor of nine when the shallow-flaw fracture-toughness K_{Ic} data set, with biaxial-loading-effects adjustments, was substituted in place of the ASME Code K_{Ic} data set in the analysis. This result indicates that incorporation of a shallow-flaw data base with biaxial loading adjustments into the PTS analysis procedures could have a significant impact on the predicted RPV failure rates. Direct application of the shallow-flaw fracture-toughness K_{Ic} data set with no biaxial-loading effects adjustment gave a much higher reduction in the conditional probability of crack initiation.

A review of the available shallow-flaw uniaxial and biaxial fracture-toughness data indicates that the biaxial loading may significantly reduce the lower-bound shallow-flaw fracture-toughness of RPV material. The biaxial-fracture-toughness curve for flaw depths of interest in a possible future proposal for modification of the P-T curve analysis procedures is located between the ASME K_{Ic} and K_{IR} curves.

The study of crack-tip constraint effects on the biaxial shallow-flaw fracture-toughness test results indicates that, (a) fracture in the shallow-flaw biaxial specimens tested at temperatures in the lower transition-temperature range is strain controlled, (b) an integral average of the opening-mode strain over the plastic zone width R_{pl} is capable of differentiating among the applied biaxial loading ratios to predict constraint-dependent $\sqrt{\delta}$ vs $\ln(R_{pl})$ loading trajectories, and (c) the parameter $\ln(R_{pl})$ can be used in a $\sqrt{\delta_c}$ or K_{Jc} vs $\ln(R_{pl})$ dual parameter fracture-toughness correlation to reflect the effect of crack-tip constraint on fracture-toughness for materials where fracture is strain controlled.

REFERENCES

1. Code of Federal Regulations, Title 10, Part 50, Section 50.61, *Fracture Toughness Requirements for Protection Against Pressurized Thermal Shock Events.*
2. U.S. Nuclear Regulatory Commission Regulatory Guide 1.154, *Format and Content of Plant-Specific Pressurized Thermal Shock Safety Analysis Reports for Pressurized Water Reactors.*
3. ASME, Boiler and Pressure Vessel Code, Section III, Division 1, Appendix G, *Protection Against Nonductile Failure.*
4. ASME, Boiler and Pressure Vessel Code, Section III, Division 1, Section NB, Subsection NB-2300, *Fracture Toughness Requirements for Materials.*
5. Code of Federal Regulations, Title 10, Part 50, Section 50.36, *Technical Specifications.*
6. U.S. Nuclear Regulatory Commission Standard Review Plan, Section 5.2.2, *Overpressure Protection,* NUREG-0800.
7. D. E. McCabe, *Evaluation of Crack Pop-Ins and the Determination of Their Relevance to Design Considerations,* NUREG/CR-5952, (ORNL/TM-12247), Martin Marietta Energy Systems, Inc., Oak Ridge National Laboratory, February 1993.
8. R. O. Ritchie, J. F. Knott, and J. R. Rice, "On the Relationship Between Critical Tensile Stress and Fracture Toughness in Mild Steel," *J. Mech. Phys. Solids*, 21, 394-410 (1973).
9. A. A. Wells, "Unstable Crack Propagation in Metals — Cleavage and Fast Fracture," Cranfield Crack Propagation Symposium, 1, September 1961, p. 210.
10. A. A. Wells, "Application of Fracture Mechnaics at and Beyond General Yielding," Report M13/63, British Welding Research Association, *British Welding Journal,* pp. 563-570, November 1963.
11. A. S. Tetelman and A. J. McEvily Jr., Fracture of Structural Materials, John Wiley & Sons, Inc., New York, 1967.
12. D. P. Clausing, "Effect of Plastic-Strain State on Ductility and Toughness," *International Journal of Fracture Mechanics* 6 (1), 71, March 1970.
13. J. M. Barsom, "Relationship Between Plane-Strain Ductility and K_{Ic} for Various Steels," *Journal of Engineering for Industry*, November 1971.
14. J. G. Merkle, *An Elastic-Plastic Thick-Walled Hollow Cylinder Analogy for Analyzing the Strains in the Plastic Zone Just Ahead of a Notch Tip,*" ORNL-TM-4071, Union Carbide Corp. Nucl. Div., Oak Ridge National Laboratory, January 1973.